Hindawi
Modelling and Simulation in Engineering
Volume 2022, Article ID 9299279, 8 pages
https://doi.org/10.1155/2022/9299279

Research Article

Absorption Performance of Doped TiO_2-Based Perovskite Solar Cell using FDTD Simulation

Budi Mulyanti,[1] **Chandra Wulandari**,[2,3] **Lilik Hasanah**,[2] **Roer Eka Pawinanto**,[1] **and Ida Hamidah**[4]

[1]*Department of Electrical Engineering Education, Universitas Pendidikan Indonesia, Bandung, 40154 Jawa Barat, Indonesia*
[2]*Department Physics Education, Universitas Pendidikan Indonesia, Bandung, 40154 Jawa Barat, Indonesia*
[3]*Engineering Physics, Institut Teknologi Bandung, Bandung, 40132 Jawa Barat, Indonesia*
[4]*Department of Mechanical Engineering Education, Universitas Pendidikan Indonesia, Bandung, 40154 Jawa Barat, Indonesia*

Correspondence should be addressed to Budi Mulyanti; bmulyanti@upi.edu

Received 18 September 2021; Revised 25 January 2022; Accepted 12 February 2022; Published 27 February 2022

Academic Editor: Noé López Perrusquia

In the third generation of the solar cell era, significant trends in the development of perovskite solar cells (PSC) were observed. Exploring suitable materials for its wafer structure, such as perovskite and electron transport layers (ETL), were a major emphasis of high-performance PSC development. Because of its matching band structure to $MaPbI_3$, TiO_2 is the most often utilized material for ETL. However, in the application of TiO_2 to PSC, electron trapping and a wide energy gap become a drawback. The goal of this research is to improve the absorption performance of PSC employing ETL with Fe and Ta-doped TiO_2 as well as the thickness of the material. The interaction between the electromagnetic waves of light and the solar cell structure was calculated using Finite-Difference Time-Domain (FDTD) simulations, which resulted in the absorption spectra. In comparison to pure TiO_2, which absorbs only 79.5% of the incident light, Fe-TiO_2 and Ta-TiO_2 as ETL in solar cells have increased absorption spectra to 81.7% and 81.2%, respectively. Finally, we may conclude that the optimum ETL layer parameters are 0.32% Fe doping and a thickness of 100 nm.

1. Introduction

Concerns about the environment, particularly the repercussions of the greenhouse effect for future generations, have prompted the development of alternative energy sources such as solar, wind, and biomass in recent decades [1]. Solar energy is regarded as the most abundant, sustainable, and ecologically beneficial renewable energy source among these [2, 3]. Because of their high efficiency of over 25%, perovskite solar cells (PSC) have attracted a lot of interest [4–8]. Perovskite is a hybrid organic-inorganic methylammonium lead halide $MaPbX_3$ ($MA = CH_3NH_3$; X = I, Br, Cr) material with excellent optoelectronic properties such as bandgap tunability, high light absorption coefficient, and long diffusion length [9, 10].

The development of PSC depends on several factors, including perovskite layer, the electron transport layer (ETL), and hole transport layer (HTL), as previously studied by Azri et al. and Hasanah et al. [11, 12]. The ETL was functioned to extract and transport the photogenerated electron and suppress the charge recombination to blocking hole as one of the significant activities in solar cell devices [13]. Therefore, the ETL is required to have high charge mobility, sufficient energy level alignment, and related morphology and interfacial properties [14]. TiO_2 is a well-known material that has widely used in PSC due to its good alignment

of conduction band to the lowest unoccupied molecular orbitals (LUMO) of active layers of perovskite [11]. However, TiO_2havea low-coordinated Ti cation at the surface, which provided electron traps due to low-lying Ti 3d and this condition reduced the charge mobility [15]. The wide energy gap owned by TiO_2limits the absorption only at the UV-light region, which can affect the PSC absorption performance [16].

The enhancement of TiO_2 properties is commonly obtained by doping with noble metal ions, transition metal, and rare metal [17]. The dopants are function to reduce the number of electron trap sites because they can replace the low-coordinated Ti cations. The charge mobility can be improved by certain amounts of dopants that trigger exciton separation[17]. TiO_2 is an n-type semiconductor, and dopants for TiO_2 are classified into two types. To begin, pentavalent cations (Nb, Ta, and so forth) increase electron conductivity in TiO_2 and thus the energy gap [18]. Second, divalent/trivalent cations (Cr, Fe, Ni, Co, and so forth) can be used to convert TiO_2 to a p-type and decrease the energy gap [19].

The absorption performance of PSC with $MaPbI_3$ was investigated in this study using different types of TiO_2 doping as ETL. Tantalum (Ta) at concentrations of 1.8% and 3.8% and iron (Fe) at concentrations of 0.11% and 0.32% were employed as dopant materials. The thickness of TiO_2-based ETL was also simulated to investigate the effect of thin and thick ETL. The simulation was obtained using Finite-Difference Time-Domain (FDTD) methods, which use Maxwell's equations to calculate. The absorption spectra are characterized at wavelengths ranging from 300 to 1500 nm, and the results are presented as absorption percentages and indexes in arbitrary units. Finally, this research should provide the best parameters for doped TiO_2-based ETL in PSC.

2. Methods

The optical model was utilized to examine the absorption performance of doped TiO_2-based PSC in this study. Lumerical Ltd.'s Finite-Difference Time-Domain (FDTD) simulations use Maxwell's equations to represent the interaction between electromagnetic light waves and the solar cell structure. FDTD simulations have been widely employed in various applications, including photovoltaic (PV) research [20]. The incident light bandwidth employed in this work was 300–1500 nm, based on an AM1.5 spectrum with a resolution of 12 nm; photon flux was high in this bandwidth but low elsewhere [21]. Light absorption is expressed as $\mathrm{Abs}(\lambda)$ for each wavelength and is formulated using

$$\mathrm{Abs}(\lambda) = \int P_{\mathrm{Abs}}(\lambda) dV. \quad (1)$$

$P_{\mathrm{Abs}}(\lambda)$ is the power absorbed per unit volume for a given wavelength, and dV is the absorber volume, which may be calculated using

$$P_{\mathrm{Abs}} = \frac{1}{2}\omega\varepsilon'' \left|\vec{E}\right|^2, \quad (2)$$

where ω is the angular frequency of the light which corresponds to the wavelength and ε'' is the imaginary part of the dielectric permittivity and $|\vec{E}|^2$ is the electric field strength.

The performance of solar cells was determined using the FDTD simulation with the refractive index as the fundamental material parameter. ITO, TiO_2, $MaPbI_3$, CuSCN, and Au were used as the front contact, electron transport layer (ETL), absorption/perovskite layer, hole transport layer (HTL), and back reflector, respectively, in the PSC structure shown in Figure 1. The earlier work [22–24] refers to these materials complex refractive index and thickness. Meanwhile, the ETL is optimized in this study by varying the doping materials and thickness. The dopants used are 1.8% and 3.8% tantalum (Ta) to produce Ta-TiO_2 and 0.11 and 0.32% iron (Fe) to produce Fe-TiO_2. The thickness was also varied to 20 nm, 50 nm, 100 nm, 200 nm, and 500 nm. The refractive index of doped TiO_2 was calculated using the refractive index-bandgap relation obtained from Reddy and Ahammed [25, 26].

The FDTD simulations are carried out in the PSC structure 2-dimensional mesh cells, with a mesh accuracy rate of 3. The light source was used in the y-axis plane-wave mode with amplitude and wavelength of 1 and 300–1500 nm, respectively. The y-axis was used with perfect matching layers (PML) and boundary conditions (BC) to maximize incident light trapping. Meanwhile, the periodic BC was applied in the x-axis, assuming the structure's infinite periodicity [27, 28]. A 2D y-normal frequency-domain field and power monitor were clamped to the layer being studied to record the absorption. The general investigation of the structure was obtained by placed the monitor between ITO-TiO_2 and CuSCN-Au. The 3D frequency-domain field and power monitor were also used to record the electric field $|\vec{E}|^2$ profile to analyze the field distribution in the PSC structure. Finally, the absorption curve and E-field profile for the desired structure and layers can be generated by this simulation.

3. Results and Discussion

3.1. Contribution of PSC Layers to Absorption Performance. As descibed in the methods,the PSC structure in this study, consists of five layers with varying materials and functions. According to Shockley-Quisser theory, the direct bandgap of $MaPbI_3$ is 1.5–1.6 eV [10]. The absorption coefficient of $MaPbI_3$ with a thickness of 280 nm was 80% of incident light in the sun-ray range [29]. As a result, these perovskite materials are an excellent candidate for absorption layer to produce high PSC performance. CuSCN with a bandgap of 3.4 eV was used in the HTL because it had the highest efficiency compared to other HTL materials such as P3HT, Spiro-OMeTAD, CuI, and NiO. The efficiency of CuSCN in HTL is supported by the excellentalignment of its highest occupied molecular orbital (HOMO) level of the CuSCN with the valence band of perovskite layer [11]. The TiO_2 with bandgap 3.2 eV used in the ETL is also used to enhance the PSC performance. Azri et al. reported that TiO_2had

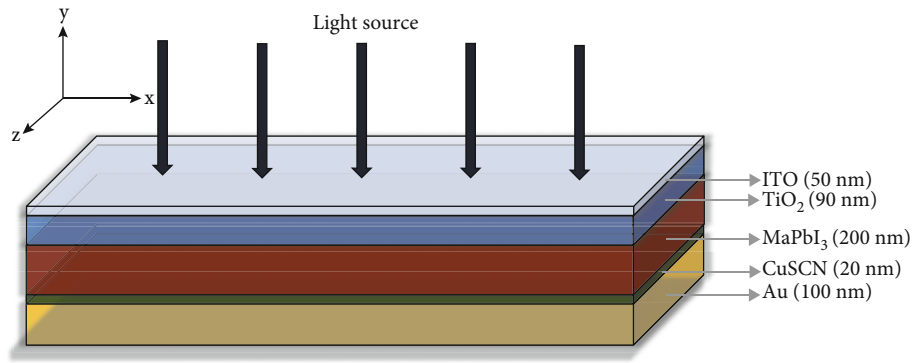

Figure 1: Sketch of PSC structure was simulated in this study; the TiO_2 layer as ETL was varied its doping and thickness.

obtained the best efficiency of 20.26% compared to ITO, PCBM, IGZO, and SnO_2 [11]. Similar to the HTL, the good ETL should have a sufficient conduction band alignment to the lowest unoccupied molecular orbitals (LUMO) of the perovskite active layers[11].

The absorption spectra for each material are simulated separately and displayed in Figure 2(a) to understand the contribution of each layer to the absorption performance of the proposed PSC structure. The gray shaded curve plane represents the absorption of the entire PSC structure, while the green, purple, red, and blue curve planes represent the absorption of each material layer, including ITO, TiO_2, $MaPbI_3$, and CuSCN. It can be seen that the $MaPbI_3$ layer contributes the most to absorption activity, which corresponds to its function as an active or absorption layer. The highest absorption reaches 0.92–0.95 at the 400–750 nm wavelength and then drops significantly to 0.1 at 800–1400 nm. On the other hand, ITO as a front contact has the lowest absorption of 0.04–0.20, indicating a suitable functionality because incident light is not trapped in the ITO and is transmitted to the active layer. TiO_2 and CuSCN have low absorption but produce a significant peak at specific wavelengths, with TiO_2 producing a peak at 312 nm and CuSCN producing a peak at 911 nm.

As can be seen, the absorption spectra collected in each layer support each other to construct the complete structural spectra. The total light absorbed by the structure reached 79.5% with an average absorption of 0.795 by examining the shorter wavelength range of 300–800 nm as shown in Figure 2(b) and assuming the white space as residual incident light from the reflectance loss. This reflectance loss is incident light that is not absorbed by the structure. We have shown in this section that TiO_2 contribution as an ETL layer is still minimal. The current study will optimize through doping and thickness modifications, and the enhancement effect will be studied by comparison in Figure 2.

3.2. Absorption Optimization using Doped TiO_2-based ETL. In this study, two contrasting characteristics of materials, namely, Ta and Fe, were used for doping variation. Ta is considered a pentavalent cation that can increase the electron conductivity in TiO_2 and robust n-type characteristics [18]. Therefore, Ta doping can be expanded the energy gap of TiO_2, namely 3.5 eV and 3.7 eV, for 1.8% Ta-TiO_2 and 3.8% Ta-TiO_2, respectively [30]. Meanwhile, Fe doping which includes divalent/trivalent cations functions to modify TiO_2 into a p-type. Fe-doped TiO_2 can decrease the bandgap from 3.2 eV to 2.76 eV and 2.68 eV for 0.11% Fe-TiO_2 and 0.32% Fe-TiO_2, respectively [19]. In this section, to discover the effect of doping in ETL, the absorption spectra were compared to pure TiO_2, as shown in Figure 3. ETL thickness was kept constant at 90 nm for each doping study.

According to Figure 3, absorption in the active layer was increased for all doping modifications. The most substantial improvement was recorded around 350 nm, 520 nm, and 911 nm. Around the wavelength of 520 nm, the doped TiO_2-based ETL achieved an absorption of 0.98. When compared to TiO_2-based ETL with 0.88 absorption, indicates 0.2 less to the maximum absorption of 1.0 and 0.1 enhancement. In terms of total light absorption, the doped ETL increased to 81.7% for Fe-TiO_2 and 81.2% for Ta-TiO_2, respectively. This finding also revealed that Fe doping is slightly greater than Ta doping, with an average absorption of 0.816 and 0.810, respectively, between 300 nm and 800 nm. Higher Fe doping performance corresponds to a reduced bandgap, and decreasing TiO_2 bandgap extends the light absorption to visible light. Lower bandgap brings the material closer to the optimal bandgap for solar cells of 1.4–2.4 eV [31]. The absorption spectra differed only slightly because of the low doping concentration in Fe-TiO_2. The results, however, showed that raising the doping concentration resulted in more significant gains.

The doping effect can also be observed from the E-field profile of PSC structure in the z-normal plane. In Figure 4, a comparison of the E-field profile for the PSC structure with ETL TiO_2 and 0.32% Fe-TiO_2 was shown. The profile in Figure 4 occurred at a certain wavelength optimum based on absorption spectra in Figure 3 including 370 nm, 516 nm, 768 nm, and 912 nm. Referring to Equation (2); the E-field $|\vec{E}|^2$ is proportional to the absorption power, P_{Abs}. The color legend shows that the color shift from deep blue to red indicates a larger E-field. For each wavelength, the E-field intensity resulting by 0.32% Fe-TiO_2-based PSC is higher than TiO_2-based PSC. With 0.32% Fe-TiO_2, the high E-field is more congregates on the front contact surface until it enters the active layer as the wavelength increases.

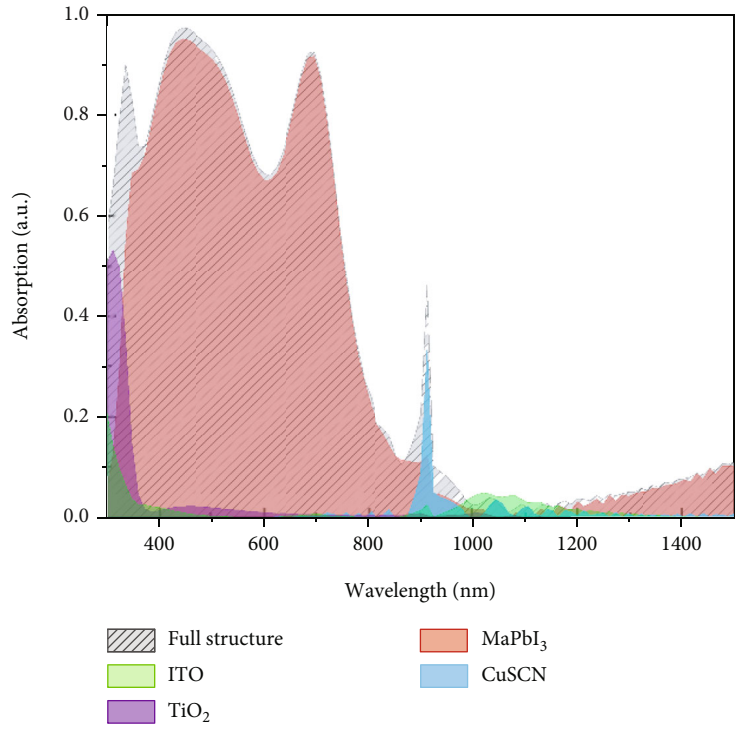

(a)

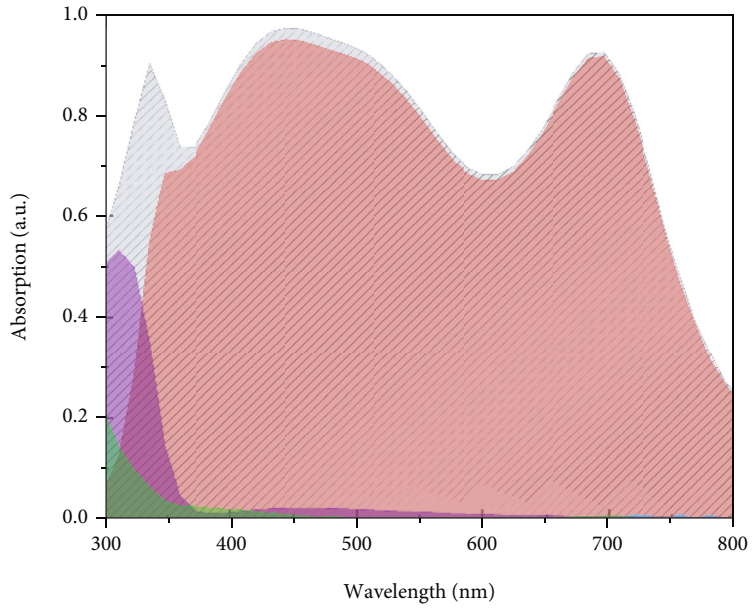

(b)

Figure 2: The spectral absorption of each layer in TiO_2-based PSC in the wavelength of (a) 300–1500 nm and (b) 300–800 nm.

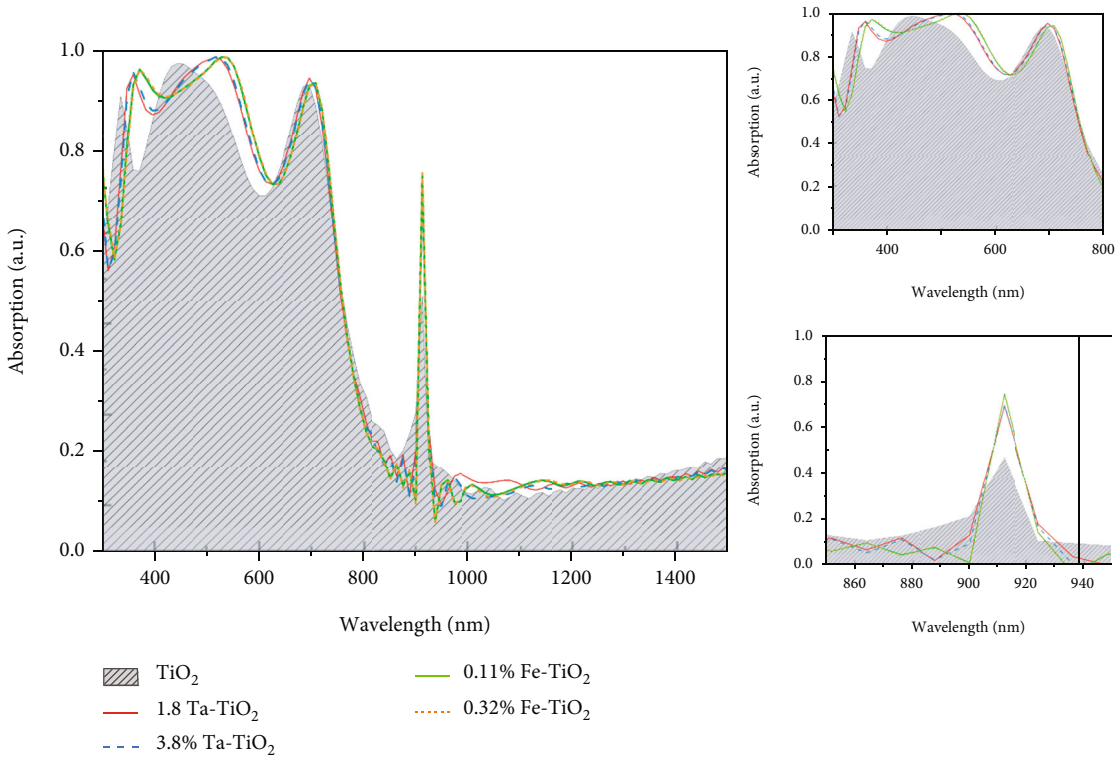

Figure 3: The spectral absorption of PSC with doping variations of TiO_2 as ETL layers.

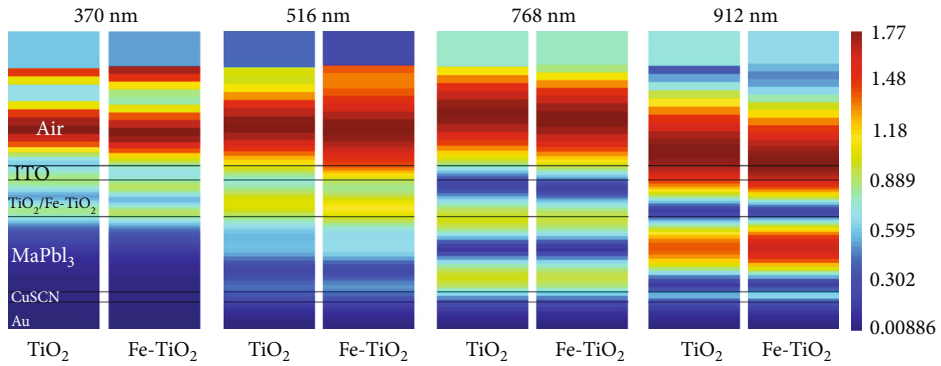

Figure 4: Comparison of *E*-field profile for PSC structure with ETL TiO_2 and 0.32% Fe-TiO_2 in wavelength of 370 nm, 516 nm, 768 nm, and 912 nm.

Generally, the light absorption in PSC can be enhanced by modifying the ETL to lead the resonance and optical enhancement. The nanostructure such as photonic crystal has been reported to result the high-performance PSC [1, 21]. Due to the strong absorption dependence on refractive index,thickness studies can also be a simple and efficient way to optimize the PSC. Tooghi et al. reported the influence of hole transport layer (HTL) thickness on the absorption, and it shows that the thinner the HTL, the better performance obtained [32]. Since the ETL was placed in front of the active layer, the thickness should not be too thick, which can block the incident light transmission nor should not be too thin to optimize the electron transport activity [32]. Several studies on PSC applied TiO_2-based ETL with thickness in the range 10–700 nm [33–37]. In this study, the thickness of 0.32% Fe-TiO_2-based ETL was varied by 20 nm, 50 nm, 100 nm, 200 nm, and 500 nm. The 500 nm ETL has a fluctuating absorption spectrum, as shown in Figure 5, indicating that incident light is reflected back into the air at certain wavelength. The thinner layer of ETL is resulting more stable absorption, but it has dropped at 650–700 nm of wavelength. The optimum absorption is provided by the 100 nm of thickness, the spectra were dropped around 750 nm, and the peak occurred around 911 nm. Finally, it can be concluded that the optimum thickness of Fe-TiO_2-based ETL is around 100 nm, with light absorption around 81%.

Finally, the proposed PSC has demonstrated excellent absorption performance. As shown in Table 1, Ta and Fe-

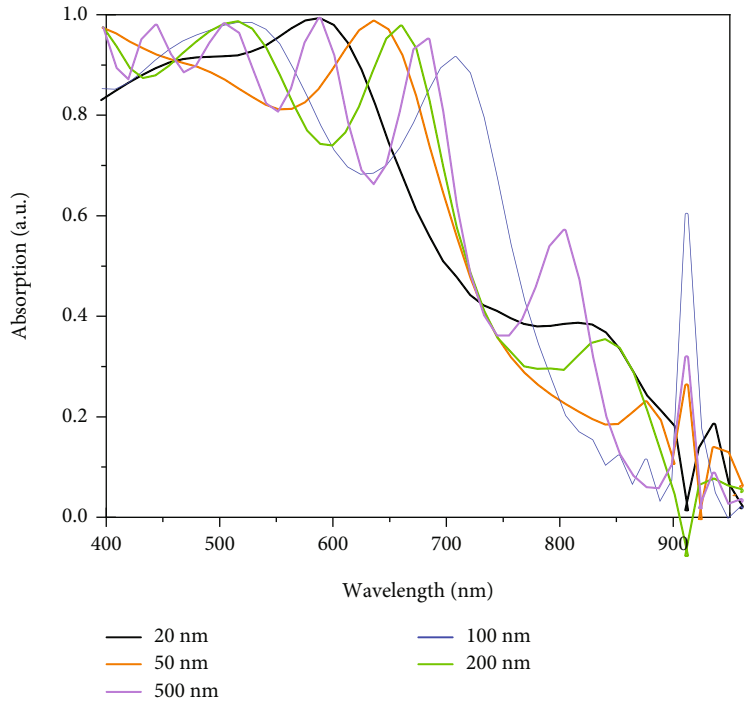

Figure 5: The spectral absorption of PSC with thickness variations of 0.32% Fe-TiO_2 as ETL layers.

Table 1: The comparison of absorption performance at 446 nm of wavelength for different TiO_2 dopant.

Structure	ETL thickness	Absorption	Reference
FTO/Er-TiO_2/$MaPbI_3$/Spiro-MeOTAD	1 μm	57%	[39]
FTO/W-TiO_2/$MaPbI_3$/Spiro-MeOTAD	5 μm	81%	[40]
FTO/Nb-TiO_2/MaPbI/Spiro-MeOTAD	40 nm	81%	[41]
FTO/Ru-TiO_2/m-TiO_2+$MaPbI_3$/Spiro-MeOTAD	50 nm	89%	[42]
ITO/Ta-TiO_2/$MaPbI_3$/CuSCN	20 nm	92%	This work
ITO/Fe-TiO_2/$MaPbI_3$/CuSCN	20 nm	92%	This work

doped TiO_2have a higher absorption percentage than other dopants reported in previous studies. Because of the higher intensity of the solar spectrum in AM1.5 [38], the comparison is specified in a wavelength of 446 nm.

4. Conclusions

In this study, the absorption enhancement of PSC-doped TiO_2 has been successfully achieved by optimizing the dopant, concentration, and thickness of ETL. The FDTD methods were used to simulate the PSC, which consist of five layers, including ITO (front contact), TiO_2 (ETL), MaPbI3 (active/absorption layer), CuSCN (HTL), and Au (back contact). The applied Fe and Ta doping into TiO_2 resulted in the higher incident light absorption of 81.7% and 81.2%, respectively, while the pure TiO_2 obtained lower absorption of 79.5%. However, the effect of doping concentrations cannot be further studied due to the slight performance difference. In general, 0.32% Fe-TiO_2 was the optimum ETL layer for the proposed PSC structure due to its ability to reduce the bandgap. The thickness optimization revealed that the thicker the ETL, the more fluctuated the spectra, and the thinner the ETL, the more the spectra dropped at short wavelength. Finally, Fe-TiO_2 with a thickness of 100 nm was concluded as the optimized ETL layers in the studied PSC. The proposed design is expected to deliver high solar cell performance in short circuit current, open-circuit voltage, fill factor, and power conversion efficiency.

Data Availability

The parameter data used to support the findings of this study are available from the corresponding author upon request.

Conflicts of Interest

The authors declare that there are no conflicts of interest regarding the publication of this paper.

Acknowledgments

The Ministry of Education and Culture of Indonesia financed this research with grant No. 278/UN40.LP/

PT.01.03/2021. The authors are grateful to Universitas Pendidikan Indonesia for providing the research facility and support.

References

[1] A. O. Salau, A. S. Olufemi, G. Oluleye, V. A. Owoeye, and I. Ismail, "Modeling and performance analysis of dye-sensitized solar cell based on ZnO compact layer and TiO_2 photoanode," *Materials Today: Proceedings*, vol. 51, pp. 502–507, 2022.

[2] M. A. Elrabiaey, M. Hussein, M. F. O. Hameed, and S. S. Obayya, "Light absorption enhancement in ultrathin film solar cell with embedded dielectric nanowires," *Scientific Reports*, vol. 10, no. 1, pp. 1–10, 2020.

[3] L. Grinis, S. Kotlyar, S. Rühle, J. Grinblat, and A. Zaban, "Conformal nano-sized inorganic coatings on mesoporous TiO_2 films for low- temperature dye-sensitized solar cell fabrication," *Advanced Functional Materials*, vol. 20, no. 2, pp. 282–288, 2010.

[4] J. Jeon, T. Eom, E. Lee et al., "Polymorphic phase control mechanism of organic–inorganic hybrid perovskite engineered by dual-site alloying," *The Journal of Physical Chemistry C*, vol. 121, no. 17, pp. 9508–9515, 2017.

[5] K. C. Ko, S. T. Bromley, J. Y. Lee, and F. Illas, "Size-dependent level alignment between rutile and anatase TiO_2nanoparticles: implications for photocatalysis," *The Journal of Physical Chemistry Letters*, vol. 8, no. 22, pp. 5593–5598, 2017.

[6] F. De Angelis, D. Meggiolaro, E. Mosconi, A. Petrozza, M. K. Nazeeruddin, and H. J. Snaith, "Trends in perovskite solar cells and optoelectronics: status of research and applications from the PSCO conference," *ACS Energy Letters*, vol. 2, no. 4, pp. 857–861, 2017.

[7] C. W. Myung, S. Javaid, K. S. Kim, and G. Lee, "Rashba–Dresselhaus effect in inorganic/organic lead iodide perovskite interfaces," *ACS Energy Letters*, vol. 3, no. 6, pp. 1294–1300, 2018.

[8] S. Javaid, C. W. Myung, J. Yun, G. Lee, and K. S. Kim, "Organic cation steered interfacial electron transfer within organic–inorganic perovskite solar cells," *Journal of Materials Chemistry A*, vol. 6, no. 10, pp. 4305–4312, 2018.

[9] B. G. Krishna, D. S. Ghosh, and S. Tiwari, "Progress in ambient air-processed perovskite solar cells: insights into processing techniques and stability assessment," *Solar Energy*, vol. 224, pp. 1369–1395, 2021.

[10] A. M. Leguy, P. Azarhoosh, M. I. Alonso et al., "Experimental and theoretical optical properties of methylammonium lead halide perovskites," *Nanoscale*, vol. 8, no. 12, pp. 6317–6327, 2016.

[11] F. Azri, A. Meftah, N. Sengouga, and A. Meftah, "Electron and hole transport layers optimization by numerical simulation of a perovskite solar cell," *Solar Energy*, vol. 181, pp. 372–378, 2019.

[12] L. Hasanah, A. Ashidiq, R. E. Pawinanto et al., "Dimensional optimization of TiO_2 nanodisk photonic crystals on lead iodide ($MAPbI_3$) perovskite solar cells by using FDTD simulations," *Applied Sciences*, vol. 12, no. 1, p. 351, 2022.

[13] H. Zhou, Q. Chen, G. Li et al., "Interface engineering of highly efficient perovskite solar cells," *Science*, vol. 345, no. 6196, pp. 542–546, 2014.

[14] G. Yang, H. Tao, P. Qin, W. Ke, and G. Fang, "Recent progress in electron transport layers for efficient perovskite solar cells," *Journal of Materials Chemistry A*, vol. 4, no. 11, pp. 3970–3990, 2016.

[15] C. H. Hsu, K. T. Chen, L. Y. Lin et al., "Tantalum-doped TiO_2 prepared by atomic layer deposition and its application in perovskite solar cells," *Nanomaterials*, vol. 11, no. 6, p. 1504, 2021.

[16] C. Xu, D. Lin, J. N. Niu, Y. H. Qiang, D. W. Li, and C. X. Tao, "Preparation of Ta-doped TiO_2using Ta_2O_5as the doping source," *Chinese Physics Letters*, vol. 32, no. 8, article 088102, 2015.

[17] J. J. Carey and K. P. McKenna, "Screening doping strategies to mitigate electron trapping at anatase TiO_2surfaces," *The Journal of Physical Chemistry C*, vol. 123, no. 36, pp. 22358–22367, 2019.

[18] V. C. Anitha, A. N. Banerjee, and S. W. Joo, "Recent developments in TiO_2 as n- and p-type transparent semiconductors: synthesis, modification, properties, and energy-related applications," *Journal of Materials Science*, vol. 50, no. 23, pp. 7495–7536, 2015.

[19] S. Larumbe, M. Monge, and C. Gómez-Polo, "Comparative study of (N, Fe) doped TiO_2 photocatalysts," *Applied Surface Science*, vol. 327, pp. 490–497, 2015.

[20] M. G. Deceglie, V. E. Ferry, A. P. Alivisatos, and H. A. Atwater, "Design of nanostructured solar cells using coupled optical and electrical modeling," *Nano Letters*, vol. 12, no. 6, pp. 2894–2900, 2012.

[21] S. Haque, M. J. Mendes, O. Sanchez-Sobrado, H. Águas, E. Fortunato, and R. Martins, "Photonic-structured TiO_2 for high-efficiency, flexible and stable perovskite solar cells," *Nano Energy*, vol. 59, pp. 91–101, 2019.

[22] L. J. Phillips, A. M. Rashed, R. E. Treharne et al., "Dispersion relation data for methylammonium lead triiodide perovskite deposited on a (100) silicon wafer using a two-step vapour-phase reaction process," *Data in Brief*, vol. 5, pp. 926–928, 2015.

[23] J. R. DeVore, "Refractive indices of rutile and sphalerite," *JOSA*, vol. 41, no. 6, pp. 416–419, 1951.

[24] P. Pattanasattayavong, G. O. N. Ndjawa, K. Zhao et al., "Electric field-induced hole transport in copper(i) thiocyanate (CuSCN) thin-films processed from solution at room temperature," *Chemical Communications*, vol. 49, no. 39, pp. 4154–4156, 2013.

[25] N. M. Ravindra, P. Ganapathy, and J. Choi, "Energy gap-refractive index relations in semiconductors - an overview," *Infrared Physics & Technology*, vol. 50, no. 1, pp. 21–29, 2007.

[26] R. R. Reddy and Y. N. Ahammed, "A study on the Moss relation," *Infrared Physics & Technology*, vol. 36, no. 5, pp. 825–830, 1995.

[27] M. J. Mendes, S. Haque, O. Sanchez-Sobrado et al., "Optimal-enhanced solar cell ultra-thinning with broadband nanophotonic light capture," *IScience*, vol. 3, pp. 238–254, 2018.

[28] M. J. Mendes, A. Araújo, A. Vicente et al., "Design of optimized wave-optical spheroidal nanostructures for photonic-enhanced solar cells," *Nano Energy*, vol. 26, pp. 286–296, 2016.

[29] C. Roldan-Carmona, O. Malinkiewicz, R. Betancur et al., "High efficiency single-junction semitransparent perovskite solar cells," *Energy & Environmental Science*, vol. 7, no. 9, pp. 2968–2973, 2014.

[30] Z. Yong, P. E. Trevisanutto, L. Chiodo et al., "Emerging giant resonant exciton induced by Ta substitution in anataseTiO_2:

a tunable correlation effect," *Physical Review B*, vol. 93, no. 20, p. 205118, 2016.

[31] I. Ramiro and A. Martí, "Intermediate band solar cells: present and future," *Progress in Photovoltaics: Research and Applications*, vol. 29, no. 7, pp. 705–713, 2021.

[32] A. Tooghi, D. Fathi, and M. Eskandari, "High-performance perovskite solar cell using photonic-plasmonic nanostructure," *Scientific Reports*, vol. 10, no. 1, pp. 1–13, 2020.

[33] W. Ke, C. C. Stoumpos, J. L. Logsdon et al., "TiO_2–ZnS cascade electron transport layer for efficient formamidinium tin iodide perovskite solar cells," *Journal of the American Chemical Society*, vol. 138, no. 45, pp. 14998–15003, 2016.

[34] X. Sun, J. Xu, L. Xiao et al., "Influence of the porosity of the TiO_2 film on the performance of the perovskite solar cell," *International Journal of Photoenergy*, vol. 2017, Article ID 4935265, 10 pages, 2017.

[35] R. Teimouri, Z. Heydari, M. P. Ghaziani et al., "Synthesizing Li doped TiO_2 electron transport layers for highly efficient planar perovskite solar cell," *Superlattices and Microstructures*, vol. 145, p. 106627, 2020.

[36] Y. Yue, T. Umeyama, Y. Kohara et al., "Polymer-assisted construction of mesoporous TiO_2layers for improving perovskite solar cell performance," *The Journal of Physical Chemistry C*, vol. 119, no. 40, pp. 22847–22854, 2015.

[37] Y. You, W. Tian, L. Min, F. Cao, K. Deng, and L. Li, "TiO_2/WO_3 bilayer as electron transport layer for efficient planar perovskite solar cell with efficiency exceeding 20%," *Advanced Materials Interfaces*, vol. 7, no. 1, p. 1901406, 2020.

[38] K. Tanabe, "A review of ultrahigh efficiency III-V semiconductor compound solar cells: multijunction tandem, lower dimensional, photonic up/down conversion and plasmonic nanometallic structures," *Energies*, vol. 2, no. 3, pp. 504–530, 2009.

[39] H. Chen, W. Zhu, Z. Zhang, W. Cai, and X. Zhou, "Er and Mg co-doped TiO_2 nanorod arrays and improvement of photovoltaic property in perovskite solar cell," *Journal of Alloys and Compounds*, vol. 771, pp. 649–657, 2019.

[40] J. Liu, J. Zhang, G. Yue, X. Lu, Z. Hu, and Y. Zhu, "W-doped TiO_2 photoanode for high performance perovskite solar cell," *Electrochimica Acta*, vol. 195, pp. 143–149, 2016.

[41] G. Yin, J. Ma, H. Jiang et al., "Enhancing efficiency and stability of perovskite solar cells through Nb-doping of TiO2at low temperature," *ACS Applied Materials & Interfaces*, vol. 9, no. 12, pp. 10752–10758, 2017.

[42] S. Wang, B. Liu, Y. Zhu et al., "Enhanced performance of TiO_2-based perovskite solar cells with Ru-doped TiO_2 electron transport layer," *Solar Energy*, vol. 169, pp. 335–342, 2018.